JACS
JOURNAL OF THE AMERICAN CHEMICAL SOCIETY

ARTICLE

pubs.acs.org/JACS

Neutral Radical and Singlet Biradical Forms of Meso-Free, -Keto, and -Diketo Hexaphyrins(1.1.1.1.1.1): Effects on Aromaticity and Photophysical Properties

Masatoshi Ishida,[†] Jae-Yoon Shin,[†] Jong Min Lim,[†] Byung Sun Lee,[†] Min-Chul Yoon,[†] Taro Koide,[‡] Jonathan L. Sessler,[*,†,§] Atsuhiro Osuka,[*,‡] and Dongho Kim[*,†]

[†]Spectroscopy Laboratory for Functional π-Electronic Systems and Department of Chemistry, Yonsei University, Seoul 120-749, Korea

[‡]Department of Chemistry, Graduate School of Science, Kyoto University, Sakyo-ku, Kyoto 606-8502, Japan

[§]Department of Chemistry and Biochemistry, The University of Texas at Austin, 1 University Station — A5300, Austin, Texas 78712-0165, United States

Supporting Information

ABSTRACT: We have investigated the electronic structures and photophysical properties of 5,10,20,25-tetrakis(pentafluorophenyl)-substituted hexaphyrin(1.1.1.1.1.1) (**1**) and its meso-keto (**2**) and meso-diketo derivatives (**3**) using various spectroscopic measurements. In conjunction with theoretical calculations, these analyses revealed fundamental structure—property relationships within this series, including unusual ground-state electronic structures with neutral, monoradical, and singlet biradical character. The meso-free species **1** is a representative 26 π-electron aromatic compound and shows characteristic spectroscopic features, including a sharp Soret band, well-defined Q-like bands, and a moderately long excited state lifetime (τ = 138 ps). In contrast, the meso-keto derivative **2** displays features characteristic of a neutral monoradical species at the ground state, including the presence of lower energy absorption bands in the NIR spectral region and a relatively short excited-state lifetime (13.9 ps). The meso-diketo **3** exhibits features similar to those of **2**, specifically NIR absorptions and a short excited-state lifetime (9.7 ps). Compound **3** is thus assigned as being a ground-state singlet biradicaloid. Two photon absorption (TPA) measurements revealed comparatively large $\sigma^{(2)}$ values of 600 GM for **2** and 1600 GM for **3** with excitation at λ_{ex} =1600 nm as compared to that observed for **1** ($\sigma^{(2)}$: 360 GM). The enhanced nonlinear optical properties of **2** and **3** are rationalized in terms of the open-shell electronic configuration allowing a large, field-induced fluctuation in the electron density (i.e., a large polarization). This interpretation is supported by theoretical evaluations of the static second hyperpolarizabilities (γ) and γ density analyses. Furthermore, nucleus-independent chemical shift (NICS) and harmonic oscillator model of aromaticity (HOMA) values and anisotropy of the induced current density (AICD) plots revealed a clear distinction in terms of the aromatic character of **1**—**3**. Importantly, the open-shell radicaloid **2** and singlet biradicaloid **3** can be formally regarded as 27 π-electron nonaromatic and 26 π-electron aromatic species, respectively, constrained within a dominant 28 π-electron conjugated network. On the basis of the combined experimental and theoretical evidence, it is concluded that the meso-carbonyl groups of **2** and **3** play an important role in perturbing the macrocyclic π-conjugation of the parent hexaphyrin structure **1**. In particular, they lead to the imposition of intrinsic radical and biradical character on the molecule as a whole and thus easy-to-discern modifications of the overall electronic effects.

I. INTRODUCTION

Aromaticity is one of the most intriguing concepts in organic chemistry. It has recently witnessed a renaissance with the appearance of conceptually new structures, including Möbius topological aromatic molecules, metal d-electron-mediated aromatic complexes, spherical shaped three-dimensional models, and so on.[1] Hückel's [4*n*+2/4*n*] rule represents one of the most successful approaches to rationalizing aromaticity from a theoretical point of view.[2] According to this rule, a flat monocyclic system with [4*n*+2]π-electrons is aromatic, whereas a planar system with [4*n*]π-electrons is antiaromatic. To date, the majority of aromatic molecules subject to detailed analysis have consisted of closed-shell cyclic systems. In contrast, the study of aromaticity effects in molecules with open-shell electronic states is still in its infancy. The concept of open-shell aromaticity was predicted by Baird,[3] who suggested that [4*n*] annulenes in their triplet π—π^* states would display aromatic character, whereas low symmetry [4*n*+2]π triplet species would prove to be antiaromatic. Subsequently, numerous theoretical studies have provided support for the notion that [4*n*]π annulene systems would be aromatic in their triplet

Received: May 20, 2011
Published: August 30, 2011

ACS Publications © 2011 American Chemical Society

states.[4] Although the synthesis of various stable radicaloid compounds has been achieved, examples of stable open-shell macrocyclic compounds suitable for testing these theoretical predictions are rare.[5] There thus remains a need for π-conjugated macrocycles with ground-state open-shell electronic configurations, including those that display neutral radical or biradical character, so as to advance our fundamental understanding of aromaticity.

Porphyrin derivatives have emerged as a promising class of the π-conjugated molecules for the investigation of aromaticity effects. These compounds, generally referred to as porphyrinoids, are also attractive for the study of radical effects. Relative to other species, porphyrinoids offer an advantage because various radical species can be stabilized by delocalization over what is usually an extended π-conjugated network (thermodynamic effect), or they may also be sterically protected by, for example, the use of meso-aryl substituents (kinetic effect), or both.[6] In fact, oxidized β,β'-doubly linked corrole dimers and a skeletally modified sapphyrin analogue in its protonated form have been recently characterized as possessing ground-state singlet biradicaloid character.[7] A stable monoradical delocalized on the bis-palladium-μ-chloride-bridged complex of a meso-aryl hexaphyrin has also been reported.[8] It has also been suggested that the meso-(di)oxygenated derivatives of 5,10,20,25-tetrakis(pentafluorophenyl)-substituted [26]hexaphyrins (1.1.1.1.1.1) (**1**) exist as stable monoradicaloid (**2**) and singlet biradicaloid (**3**) species in their respective ground states (Chart 1).[9] This makes the series **1**−**3**, along with the reduced 28 π-electron congener of **1** (species **4**: Chart 1), of particular interest in terms of studying aromaticity effects in open-shell porphyrinoid species. In this Article, we detail the combined use of spectroscopic and theoretical methods in the analysis of two particular open-shell systems, **2** and **3**.

Meso-free hexaphyrin **1** has pentafluorophenyl substituents at four of the six meso-positions. These substituents point outward from the center of the ring, while the other two meso-positions, which bear no substitutents, face inward. Presumably, because it lacks two meso substituents relative to all meso-substituted hexaphyrin(1.1.1.1.1.1) (**5**), compound **1** displays unique reactivity at its free meso-positions.[10] Specifically, the meso-oxygenated keto hexaphyrin **2** may be formed from **1** via C−H oxygenation. In further contrast to what is true for fully substituted meso-aryl hexaphyrins, such as **5**, the bis meso-free system **1** also displays unique metal coordination chemistry, including cation complexation that is accompanied by inner meso C−H oxygenation.[11] In the specific case of reaction with the nickel(II) cation, two metal ions were accommodated in a square planar coordination environment, wherein the pyrrolic nitrogen atoms and the carbonyl oxygen atoms resulting from oxygenation stabilize the bis-nickel(II) complex; acid-catalyzed demetalation then allowed for isolation of the dioxygenated meso-diketo hexaphyrin derivative **3**.[9b] On the basis of various spectroscopic, electrochemical, and magnetic susceptibility measurements carried out in the previous studies, the mono oxygenated derivative **2** was considered to be a neutral radicaloid species whose unpaired electron is delocalized with the macrocyclic π-electron periphery. On this same basis, the doubly oxygenated species **3** was considered to be a singlet biradicaloid in the ground state. Interestingly, despite their radical or radicaloid character, both **2** and **3** exhibit high chemical stability under ambient conditions. This makes these two hexaphyrin derivatives attractive open-shell systems with which to study aromaticity effects. Both of these compounds, like the parent system **1**, are characterized by planar Type I dumbbell-like conformations; this, it was thought, would allow for cleaner intercomparisons.

Chart 1. Molecular Structure of (a) Meso-Free [26]Hexaphyrin 1, (b) Meso-Keto Derivative 2, (c) Meso-Diketo Derivative 3, (d) Meso-Free [28]Hexaphyrin 4, and (e) Meso-Aryl [26]Hexaphyrin 5 Used in This Study[a]

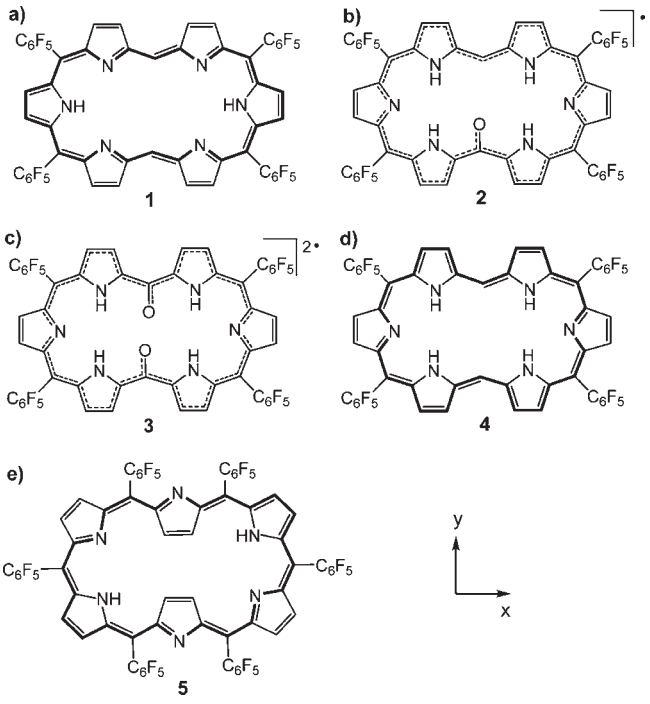

[a]The C_6F_5 designation refers to the 2,3,4,5,6-pentafluorophenyl group.

In an effort to understand further the influence of radical character on various discernible aromaticity effects, we have carried out a detailed analysis of the photophysical properties of **1**−**3** using steady-state electronic and vibrational spectroscopies, ultrafast time-resolved spectroscopies, and femtosecond *z*-scan measurements. Supporting theoretical calculations with spin-unrestricted density functional theory (UDFT) were also carried out to define the intrinsic nature of neutral radical and singlet biradical systems in their open-shell configurations. Static second hyperpolarizability (γ) calculations were likewise made with a view to rationalize the observed third-order NLO properties. The scientific question we sought to address through this combined body of theory and experiment is how these particular open-shell radical and singlet biradical macrocyclic systems can be treated under the general $[4n+2/4n]$ aromaticity rule. Although the original nonoxygenated hexaphyrin **1** is easily recognized as being a Hückel aromatic 26π-electron conjugated porphyrinoid based on previously reported experimental findings, a priori it appeared difficult to characterize the open-shell species **2** and **3** with regard to their electronic features. On the basis of NICS and HOMA values, ^{1}H NMR chemical shifts, and AICD calculations, we now propose that the monoradical **2** and singlet biradicaloid **3** should be formally regarded as open-shell nonaromatic and aromatic macrocyclic species, respectively, according to the Hückel (or Baird) rule.

II. EXPERIMENTAL SECTION

Materials and Instruments. Unless noted otherwise, chemicals of the best possible grade were purchased from commercial suppliers and were used without further purification. Details of the preparation, characterization, and the X-ray crystallographic analyses of **1**, **2**, and **3** have been previously published.[9] UV−vis−NIR absorption spectra were recorded with a Varian Cary-5000 UV−vis−NIR spectrometer, and fluorescent spectra were recorded on a Shimadzu RF-2500 fluorometer. A quartz cell with an optical path length of 10 mm was used for all of the steady-state measurements. Fourier transform infrared spectra of solid samples were measured on a Bruker VERTEX 70 FTIR spectrometer using a KBr pellet.

Femtosecond Transient Absorption Measurements. The femtosecond time-resolved transient absorption (TA) spectrometer used for this study consisted of a homemade noncollinear optical parametric amplifier (NOPA) pumped by a Ti:sapphire regenerative amplifier system (Quantronix, Integra-C) operating at 1 kHz repetition rate and an accompanying optical detection system. The generated visible NOPA pulses had a pulse width of ∼100 fs and an average power of 1 mW in the range 450−800 nm, which were used as pump pulses. White light continuum (WLC) probe pulses were generated using a sapphire window (2 mm thick) by focusing of small portion of the fundamental 800 nm pulses, which were picked off by a quartz plate before entering into the NOPA. The time delay between pump and probe beams was carefully controlled by making the pump beam travel along a variable optical delay (Newport, ILS250). Intensities of the spectrally dispersed WLC probe pulses were monitored by miniature spectrograph (OceanOptics, USB2000+). To obtain the time-resolved transient absorption difference signal (ΔA) at a specific time, the pump pulses were chopped at 25 Hz and absorption spectra intensities were saved alternately with or without pump pulse. Typically, 6000 pulses were used excite samples and to obtain the TA spectra at a particular delay time. The polarization angle between pump and probe beam was set at the magic angle (54.7°) using a Glan-laser polarizer with a half-wave retarder to prevent polarization-dependent signals. The cross-correlation fwhm in the pump−probe experiments was less than 200 fs, and chirp of WLC probe pulses was measured to be 800 fs in the 400−800 nm region. To minimize chirp, all reflection optics were used in the probe beam path, and a quartz cell of 2 mm path length was employed. After completing each set of fluorescence and TA experiments, the absorption spectra of all compounds were carefully checked to rule out the presence of artifacts or spurious signals arising from, for example, degradation or photo-oxidation of the samples in question.

Two-Photon Absorption Experiments. Two-photon absorption (TPA) spectra were measured in the NIR region using the open-aperture *Z*-scan method with 130 fs pulses from an optical parametric amplifier (Light Conversion, TOPAS) operating at a repetition rate of 3 kHz generated from a Ti:sapphire regenerative amplifier system (Spectra-Physics, Hurricane-X). The NIR beam was divided into two parts. One was monitored by a Ge-PIN photodiode (New Focus) as an intensity reference, and the other was used for the transmittance measurement. After passing through a 10 cm focal length lens, the laser beam was focused and passed through a 1 mm quartz cell. Because the position of the sample cell could be controlled along the laser beam direction (z axis) using a motor-controlled delay stage, the local power density within the sample cell could be controlled simply under constant laser intensity. The transmitted laser beam from the sample cell was then detected by the same photodiode as used for reference monitoring. The on-axis peak intensity of the incident pulses at the focal point, I_0, ranged from 40 to 60 GW cm^{-2}. For a Gaussian beam profile, the nonlinear absorption coefficient can be obtained by curve fitting of the observed open-aperture traces $T(z)$ with the following equation:

$$T(z) = 1 - \frac{\beta I_0 (1 - e^{-\alpha_0 l})}{2\sqrt{2}\alpha_0 [1 + (z/z_0)^2]}$$

where α_0 is the linear absorption coefficient, l is the sample length, and z_0 is the diffraction length of the incident beam. After the nonlinear absorption coefficient has been obtained, the TPA cross section $\sigma^{(2)}$ of one solute molecule (in units of GM, where 1 GM = 10^{-50} cm^4 s photon^{-1} molecule^{-1}) can be determined by using the following relationship:

$$\beta = \frac{10^{-3}\sigma^{(2)} N_A d}{h\nu}$$

where N_A is the Avogadro constant, d is the concentration of the compound in solution, h is the Planck constant, and ν is the frequency of the incident laser beam. We obtained TPA spectra with a 50 nm step for **1**−**3** at 1600 nm, where linear absorption is negligible, to satisfy the condition of $\alpha_0 l < 1$ in retrieving the pure TPA values $\sigma^{(2)}$ in the simulation procedure. We also measured a value of 900 GM at 1200 nm for the TPA cross section of the reference compound Styryl 9M.[12]

Theoretical Calculations. All calculations reported in this study were carried out using the Gaussian 03 program package.[13] Full optimization of the structure of the meso-free [26]hexaphyrin **1** and its antiaromatic congener of **1**, [28]hexaphyrin (**4**), which is used as a comparable model for **2** and **3** (vide infra), was performed using Becke's three-parameter hybrid exchange functional and the Lee−Yang−Parr correlation functional (B3LYP)[14] employing the 6-31G(d,p) basis set. Analyses of the meso-keto **2** and diketo **3** derivatives were performed using the spin-unrestricted B3LYP (UB3LYP) method. The singlet biradical state of **3**, in particular, was calculated using the broken-symmetry UB3LYP method. Some calculations performed in an effort to simulate the vibrational frequencies, NICS values, and create plots of the AICD were carried out using model systems in which all pentafluorophenyl substituents were replaced with hydrogen atoms. In the calculation of the second hyperpolarizability (γ) and hyperpolarizabity density, the computational procedure was carried out in accord with the method proposed by Nakano and co-workers.[15] Following their method, the longitudinal component of the second hyperpolarizability (γ_{xxxx}) was calculated; this was done because the component along the x-axis is expected to dominate in terms of reflecting the π-electron delocalization (Chart 1). For a finite field calculation of γ, Becke's half and half LYP (BHandHLYP) method was employed using the 6-31G (d) basis set. This allowed us to take advantage of reliable γ values for single biradical molecules as reported previously. The γ densities were calculated for a grid of points using a numerical third-order differentiation formula for the electron densities. The box dimensions (-12 Å $\le x \le 12$ Å, -10 Å $\le y \le 10$ Å, -5 Å $\le z \le 5$ Å) were chosen to ensure that the γ values obtained by integration are within 5% of the finite field results.

III. RESULTS AND DISCUSSION

Structural Geometries and Theoretic Analyses. While the ordinary meso-aryl-substituted [26]hexaphyrin **5** exhibits a planar rectangular shape (Type II conformation), the conformations of the hexaphyrin derivatives **1**, **2**, and **3** are nearly dumbbell-shaped (Type I conformation), as inferred from X-ray crystallography (Chart 1). The central cores of **1** and **2** are characterized by relatively high planarity (the mean plane deviation: d_{mean} = 0.109 Å for **1** and 0.211 Å for **2**, respectively), whereas the core of **3** is somewhat folded at the center of the macrocycle (d_{mean} = 0.232 Å), presumably because of steric

Table 1. Structural Information for the Hexaphyrin Derivatives 1−4

sample	d_{mean}[a] (Å)	d_{mean}[b] (Å)	$\nu_{C=O}$[c] (cm^{-1})	$\nu_{C=O}$[d] (cm^{-1})	NICS(0)[b] (ppm)	HOMA[b]	energy gap[e] (eV)
1	0.109	0.084			−15.1	0.844	1.88
2	0.211	0.287	1564	1645	+4.2	0.731	1.40 (α-spin)
3	0.232	0.219	1574	1649	−8.2	0.672	1.45 (both spin)
4		0.220			+43.1	0.653	1.09

[a] Derived from the X-ray crystal structures. [b] Derived using the optimized structures. [c] Observed in the FTIR spectrum. [d] Determined from the frequency calculations with the meso-aryl substituents omitted. [e] HOMO(SOMO)−LUMO energy as obtained from (U)DFT calculations.

hindrance between the central carbonyl groups and the neighboring pyrrolic NH protons (Table 1). In the DFT optimized structures, compounds **1**, **2**, and **3** demonstrated conformational features similar to those seen in the solid state and determined by single crystal X-ray diffraction analysis (Figure S1 in the Supporting Information). The mean plane deviations, d_{mean}, of the optimized structures are 0.084 Å for **1**, 0.287 Å for **2**, and 0.219 Å for **3**, respectively (Table 1). The structure of **2** obtained from the DFT optimization process seems to be relatively distorted in comparison with the structure derived from the crystallographic data as judged from an increase in the deviation value. The difference between the experimental and theoretical results is ascribed to intrinsic packing effects and associated restriction on the geometry of **2** imposed in the crystal lattice (Figure S2 in the Supporting Information).

A comparison of selected bond lengths (Å) and angles (degrees) derived from the crystal and optimized (calculated) structures is presented in Tables S1, S2, and S3 in the Supporting Information. Using both restricted and unrestricted B3LYP methods, the bond lengths and angles of the core hexaphyrin frameworks of **1**, **2**, and **3** determined from the calculations proved to be in good agreement with the experimental results. In particular, the bond lengths of the characteristic carbonyl C═O moieties obtained in the optimized structures of **2** and **3** are 1.248 and 1.237 Å, respectively, which are also in agreement with those of the crystal structures (1.281 and 1.223 Å for **2** and **3**, respectively). On the basis of these optimized carbonyl bond lengths, it was inferred that the C═O bond of **3** has greater double bond character than the carbonyl moiety present in **2**. Thus, because various possible resonance forms for **3** include an oxyallyl unit (Scheme S1 in the Supporting Information), it is important to note that based on geometric considerations the central C═O groups are carbonyl-like in terms of their overall chemical character.

To gain further insight into the structural differences between **2** and **3**, particularly with regard to the electronic character of the C═O moiety, the carbonyl stretching features of **2** and **3** were probed via infrared (IR) spectroscopy. Features at 1564 and 1574 cm^{-1} were seen in the FTIR spectra recorded using a KBr pellet in the case of **2** and **3**, respectively (Figure 1).[16] These values are consistent with the $\nu_{C=O}$ = 1583 cm^{-1} recorded for a meso-di(pentafluorophenyl) diketo-bridged dipyrrin derivative.[17] The 1564 and 1574 cm^{-1} features seen for **2** and **3** were thus assigned to C═O stretching frequencies ($\nu_{C=O}$) and provide support for the conclusion that both **2** and **3** contain meso-carbonyl moieties with double bond C═O character. Nevertheless, the 10 cm^{-1} shift to lower energy seen in **2** as compared to **3** leads us to suggest that there is a reduction in the C═O bond order (reduced double bond character) in the case of **2**, as was inferred from the

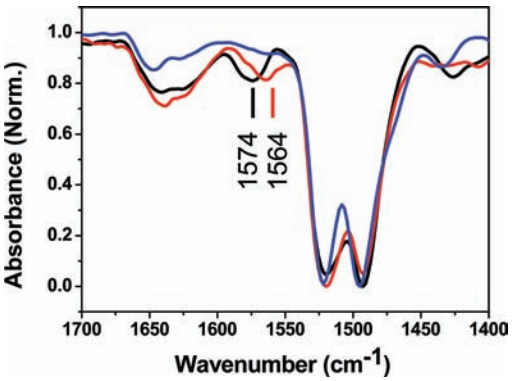

Figure 1. FTIR spectra of **1** (blue line), **2** (red), and **3** (black) showing the 1400−1700 cm^{-1} spectral region. The assigned C═O stretching vibrations for **2** and **3** are indicated along with the corresponding wave numbers. See text for the basis of the mode assignments.

structural parameters including the calculated bond order trends (vide supra).

Further support for the above mode assignment came from DFT calculations. Specifically, the FTIR spectral features in **2** and **3** could be simulated via unrestricted DFT frequency calculations. The eigenvectors of the corresponding C═O vibrations represent the $\nu_{C=O}$ bands at 1645 cm^{-1} for **2** and 1649 cm^{-1} for **3**, respectively; they thus follow the same trend as above with a small dispersion value.[18] The decreased C═O bond nature of **2** inferred from this combination of experiment and theory may reflect a degree of resonance involving contributions from enol-like structures and conjugation with the tripyrrane subunits. However, the effect of this conjugation is minor, and the carbonyl C═O moieties in both **2** and **3** retain overall double bonded character as observed in the IR measurements and inferred from the structural parameters, as noted above. The dominance of this keto form, in turn, interferes with the macrocyclic π conjugation as a whole and is considered to be one key determinant leading to the observed ground-state radical and biradical character observed in the case of **2** and **3**, respectively.

Steady-State Optical Properties and DFT Simulated Transitions. The steady-state absorption spectrum of **1** in toluene exhibits a spectral pattern typical of aromatic expanded porphyrins, as shown in Figure 2a. A sharp, intense Soret (B-)-like band is observed at 553 nm along with Q-like bands in the near-infrared (NIR) region that are characterized by their clear vibronic structures. These distinct spectral features seen in the case of **1** are similar to those observed for other meso-aryl-substituted [26]hexaphyrins, such as **5** (Chart 1). This concordance is thus consistent with the proposed aromatic character ascribed to **1**, a species that we think should be considered as being 26 π-electron

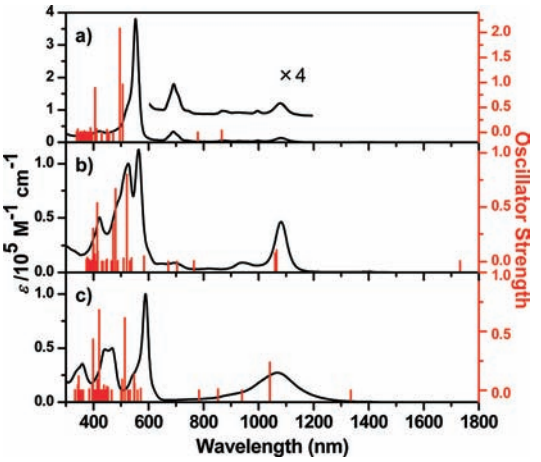

Figure 2. Steady-state absorption spectra (black) and calculated vertical excitation energies (red) of (a) **1**, (b) **2**, and (c) **3**.

macrocycle with a highly symmetric molecular structure.[19] In contrast, the absorption spectrum of **2** shows split B-like bands at 442, 526, and 564 nm. A relatively intense peak at 1082 nm is also seen in what is an unusually low energy region in which to observe Q-like bands, particularly in the case of hexaphyrins. The absorption spectrum of **3** also exhibits a broad, low energy absorption feature at 1069 nm, along with B-like bands at 360, 442, 468, and 589 nm.

To assign the unique spectral features observed in the presumed radicaloid species, **2** and **3**, vertical excitation energies were calculated using the time-dependent (TD)-DFT method employing spin restricted and unrestricted (U)B3LYP/6-31G(d, p) basis sets for **1**, **2**, and **3**, respectively (Figure 2). The simulated electronic states of **1**, **2**, and **3** were found to match well with the experimental spectra with respect to both position and relative intensity.[20] The electronic transitions of **1** can be explained readily using Gouterman's four-orbital model for tetrapyrrolic macrocycles and other aromatic hexaphyrins.[21] Specifically, the B-like and two Q-like bands are generated by configuration interactions between the four frontier molecular orbitals (MOs): HOMO−1(a_u), HOMO(b_{1u}), LUMO(b_{2g}), and LUMO+1(b_{3g}) (Figure S4 and Table S4 in the Supporting Information). On the other hand, the vertical transitions of **2** proved more difficult to treat due to their open-shell electronic configurations. However, transition features that are overall consistent with the experimental spectra, including the corresponding NIR transitions and the three allowed intense transitions in the visible region, could be modeled. Importantly, a lowest excited state at 1732 nm with very weak oscillator strength (f = 0.0061), which corresponds to a direct transition from α-SOMO to α-LUMO of **2**, was predicted (Figure S5 and Table S5 in the Supporting Information) but not experimentally observed. This lowest energy excited state is ascribed to a one-photon optically forbidden state, which has been observed in other Hückel antiaromatic expanded porphyrins (e.g., [28]hexaphyrin).[19,22] The lowest energy peaks actually seen in the absorption spectrum are thus assigned to SOMO−LUMO and SOMO−LUMO+1 transitions involving β-spins. Overall, the transition features of **2** are in agreement with what was observed for a μ-chloro bis(palladium) hexaphyrin complex displaying monoradical character.[8] This provides support for the proposed assignments.

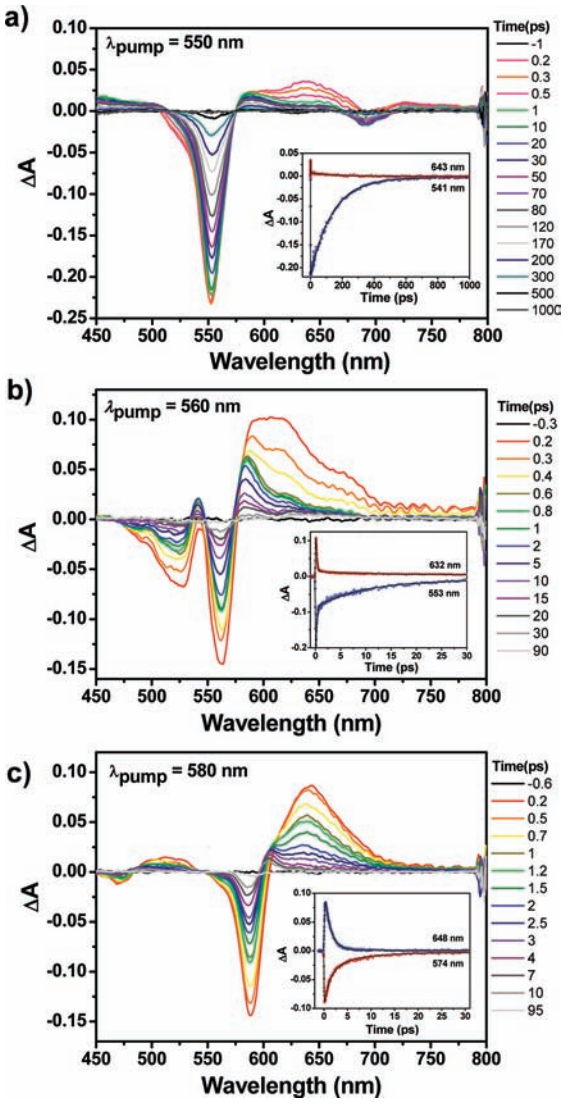

Figure 3. Transient absorption spectra of (a) **1**, (b) **2**, and (c) **3** recorded in toluene. The inset shows the decay profiles. λ_{ex} = 550 nm for **1**, 560 nm for **2**, and 580 nm for **3**, respectively.

In the case of **3**, the lowest predicted spectral feature (at 1335 nm) was also assigned to a transition involving a one-photon forbidden state with nearly zero-oscillator strength (Figure S6 and Table S6 in the Supporting Information). The first excited state arises from HSOMO−LUMO transitions of both α- and β-spins, which is likewise attributed to an optically forbidden transition. The configuration interaction of this transition is indeed similar to that of the lowest-energy transition simulated in the case of **2**, as well as for the previously reported oxidized corrole dimers.[7b] The NIR band observed in the spectrum of **3** could be modeled as a second one-photon allowed transition, which is derived from the admixture of dominant HSOMO−LUMO transitions with a minor contribution from SOMO−1−LUMO+1 transitions. On this basis, we suggest that the lowest energy band seen in the absorption spectra of **3** has its origin in several complicated, albeit optically allowed, transitions with the second predicted transition underlying the primary excited state. This rationale, to the extent it is true, presumably reflects the open-shell configuration, which leads to a greater

number of configuration interactions and gives rise to a large number of excited states. In this respect, the complex optical features of **2** and **3** can be considered to reflect their proposed radicaloid character.

Excited-State Dynamics. Femtosecond transient absorption (TA) measurements were carried out to explore the extent to which the open-shell electronic structure affected the excited-state photophysical properties of **2** and **3** (Figure 3). In the TA spectrum of **1**, sharp and intense ground-state bleach (GSB) signals around 560 nm are observed that are accompanied by weak excited-state absorption (ESA) bands in 450−500 and 570−670 nm spectral regions. The dynamic spectral features of **1** are typical of those observed for aromatic [26]hexaphyrin systems.[19] In contrast, the TA spectra of **2** and **3** exhibit relatively strong ESA signals and weak GSB features. Time-dependent TA spectral changes, characterized by a slight blue shift in the ESA signals, were noted in the case of both **2** and **3**; these shifts were readily apparent at ca. 0.8−1 ps (for **2**) and 3−4 ps (for **3**) after photoexcitation. These blue shifts and an accompanying peak contraction in the observed ESA signals for **2** and **3** could reflect conformational/vibrational relaxation processes.[23] These processes in the excited vibrational state from the higher excited singlet state (S_n) might be attributable; further analyses will be, however, needed before this assignment is fully secure in the case of the open-shell electronic systems, **2** and **3**.

The excited-state lifetimes of **1** and **2** (138 and 13.9 ps) were reported previously.[9a] The singlet excited-state lifetime of **1** is typical as compared to that of meso-aryl aromatic [26]hexaphyrins with Type II conformation (98 ps).[19] This decay profile of **1** is reasonable by taking into account the characteristic aromatic character, while the doublet excited-state lifetime of **2** is much shorter. By detailed monitoring of the change in the ESA signals as a function of time, the decay profiles of **2** and **3** could be fit to a double exponential. This fitting revealed ultrafast (∼1 ps) and relatively short (9−13 ps) time components, which are similar to the kinetic features of antiaromatic expanded porphyrins with a so-called "optically dark state".[22] In this prior work, the reduced lifetime of **2** (relative to **1**) was ascribed to a high density of states (arising from the radical nature of **2**), which served to stimulate energy relaxation through internal conversion processes. In fact, according to the TD-DFT calculations mentioned above, there is an one-photon forbidden state (optically dark state), between the lowest optically allowed state and the ground state.[22] Although this low-lying, optically dark state could not be observed in the absorption spectrum, it can act as a ladder state in the energy relaxation processes. Specifically, we propose that the lowest Q-like state of **2** is depopulated within 1 ps to the optically dark S_1-state. This dark state decays to the ground state via internal conversion and does so with a relatively short excited-state lifetime of 13.9 ps, in accord with the energy-gap law.

The excited-state lifetime of **3** was estimated to be 9.7 ps from the TA decay profiles (Figure 3c). This ultrafast decay time is comparable to that of **2** and, again, is ascribed to the presence of an optically dark state located in the lower energy spectral region. As might be expected, the TA spectral features of **2** and **3** differ noticeably from those of **1**. In the event, it is important to note that the TA spectra of the open-shell species **2** and **3**, especially their respective ESA signals, differ from those of **1**. This lack of congruence is thought to reflect excited states with a very different character. In particular, the TA signals of **2** and **3** are thought to reflect the presence of an one-photon forbidden excited state that provides a rapid nonradiative channel for excited-state deactivation, while the TA signals of **1** reflect population of a one-photon allowed excited state. The nonfluorescent properties of **2** and **3** are also consistent with their short excited-state lifetimes and are considered to reflect an acceleration of the nonradiative internal conversion rates from the S_1 to the S_0 state arising from their relatively reduced energy gaps.

A detailed comparison of ultrafast decay time profiles for **2** (0.2 ps) and **3** (1.2 ps) allows subtle differences to be noted. Specifically, a distinctive depopulation of the initial excited state to produce an optically dark state with longer energy relaxation dynamics was seen in the case of **3**. The longer first kinetic decay profile seen for **3** relative to **2** is thought to reflect differences in their respective electronic character that are manifest in terms of distinct transition selection rules, excited-state energies, and dynamics (vide infra).

Enhancement of Two-Photon Absorption Properties in the Radicaloid 2 and Singlet Biradicaloid 3. We have already reported the TPA properties of various porphyrin derivatives including the expanded porphyrinoids with relatively large TPA cross section values. As a general rule, we have found that the third-order NLO response reflects variations in the electronic structure as well as the conformational geometry of the molecules, giving rise to the underlying static and dynamic polarizability.[24] In contrast with the closed-shell systems that have been the subject of study to date, the neutral radical **2** and singlet biradical **3** possess unusual ground-state structures characterized by open-shell configurations. They thus represent a new class of substrates whose study could lead to an improved understanding of TPA structure−function correlations.

The TPA cross-section values of **1**−**3** were measured using the femtosecond *z*-scan method and a low energy two-photon excitation wavelength (λ_{ex} = 1600 nm) where one-photon absorption contributions to two-photon absorption can be ignored (Table 2 and see Figure S7 in the Supporting Information). The TPA cross section ($\sigma^{(2)}$) of the closed-shell system **1** was determined to be 360 GM. This value is comparable to those recorded for other meso-aryl-substituted [26]hexaphyrins. The keto hexaphyrin **2** exhibited a somewhat larger TPA cross section value of 600 GM as compared to **1**, a finding that leads us to suggest that the monoradical character of **2** contributes to the observed TPA cross-section values, as was suggested in the case of a previously studied radical palladium hexaphyrin complex.[8] The diketo hexaphyrin **3** exhibited an even larger TPA cross section value of 1600 GM. This is consistent with its proposed diradical character as mentioned below.

It has been already demonstrated that benzene- and naphthalene-bridged bis(phenalenyl) hydrocarbons with intermediate singlet biradical character display relatively large TPA values, 424 GM at λ_{ex} = 1425 nm and 890 GM at λ_{ex} = 1500 nm, respectively.[25] On the basis of this experimental result, Nakano et al. have proposed a structure−property relationship for the second hyperpolarizability (γ), which is a distinct molecular property that contributes to the third-order NLO response in phenalenyl radical systems.[15,26] Specifically, it was suggested by these researchers that other singlet biradical systems with intermediate diradical character should show a significant enhancement in the γ values depending on the spin multiplicities.[27] In the event, it is inferred that singlet biradical molecules would be good candidates in which to show tunable NLO susceptibilities because of the feasibility of controlling the hyperpolarizability.

To further deepen our understanding of these predictions and apply them to an analysis of the TPA enhancements seen in **2** and

Table 2. Photophysical Data, TPA Cross Sections, and Static γ Values for the Derivatives, 1−3

sample	λ_{max}[a] B-like bands (nm)	λ_{max}[a] Q-like bands (nm)	λ_{max}[a] NIR band (nm)	τ_{S1}[b] (ps)	$\sigma^{(2)c}$ (GM)	γ_{xxxx}[d] (10^3 au)
1	533	690, 868, 997	1079	138(100)	360	23
2	422, 526, 564	694, 940	1082	0.2(72), 13.9(28)	600	126
3	360, 442, 468		1069	1.2(81), 9.7(19)	1600	883

[a] Absorption maxima in toluene solution. [b] Observed in the ground-state bleaching; values in parentheses are percentages of the total amplitude. [c] Excitation wavelength; λ_{ex} = 1600 nm. [d] Calculated dominant longitudinal components.

3, theoretical analyses of the static second hyperpolarizability (γ) of **1**−**3** were carried out. A γ density calculation was also run in an effort to clarify the spatial contribution of the electron density to the γ values.[26] Here, positive and negative γ densities correspond to field-induced increases and decreases in the third-order charge density, leading to the third-order dipole moment (third-order polarization) in the direction from positive to negative γ density. Therefore, the γ density map represents the relative phase and magnitude change in the third-order charge densities between two spatial points with positive and negative γ densities.

The longitudinal components of the static γ (γ_{xxxx}) values were calculated using the finite field (U)BHandLHYP/6-31G* method for **1** (singlet), **2** (doublet), and **3** (singlet), as shown in Table 2. The γ values of the open-shell system **2** ($\gamma = 126 \times 10^3$ au) and **3** ($\gamma = 883 \times 10^3$ au) are about 5 and 40 times larger than that of **1** ($\gamma = 23 \times 10^3$ au), respectively. The significant enhancement in the γ values for **2** and **3** relative to that of **1** is consistent with the trend in the TPA cross-section values. Specifically, the radicaloid and biradicaloid electronic structures tend to exhibit larger γ values than the closed-shell systems with similar π-conjugated frameworks. Furthermore, the γ density distributions for **1**−**3** provide support for the notion that the main contributions arise from the π-electrons but that the σ-electrons do provide smaller contributions to the γ value in all three derivatives (Figure 4). In the case of **1**, the γ density was found to be small and uniformly distributed as would be expected for a 26π-electron conjugated system.

In contrast to what was seen for **1**, extended positive and negative γ densities were noted in **3**; these were found to be separately distributed on the left- and right-hand tripyrrane units. It has been suggested that ground-state singlet biradical molecules with intermediate diradical character, specifically those with a y index of around 0.38 (the y index is a value between 0 [closed-shell state] and 1 [pure biradical state]), will display a maximal third-order NLO response, including TPA activity.[28] This parameter is a reflection of bond dissociation, meaning that intermediate biradical species are those with $0 < y < 1$. Species with intermediate y indices (and the attendant partial bond breaking) are characterized by large, facile fluctuations in their valence electrons under an applied electric field. In other words, in the presence of an applied external field, intermediate biradical molecules display "soft" electronic structures in comparison with appropriate closed-shell or pure diradical control systems. We also estimated the γ of **3** with closed-shell (CS: $y = 0$) and open-shell triplet (TS: $y = 1$) configurations using the (U) BHandHLYP finite field approach so as to obtain insights into spin multiplicity effects. On this basis, the γ values of **3**(CS) and **3**(TS) were determined to be 48 × 10^3 and 220 × 10^3 au, respectively. This result provides support for the reasonable supposition that it is the intermediate singlet biradical character of **3** that leads to the greater enhancement in the γ value (almost 4−20 times larger) with respect to the corresponding closed-shell and pure diradical systems. The decreased γ value seen in the closed-shell and triplet states is consistent with what has been observed previously in the case of a phenalenyl radical system.[27] Using the following equation, the y value was evaluated by various experimental parameters, such as the energy of the lowest one- and two-photon absorption bands and the lowest triplet excited state:[29]

$$y = 1 - \sqrt{1 - \left(\frac{^1E_{1u}, s_{1g} - {}^1E_{1u}, s_{1g}}{^1E_{2g}, s_{1g}} \right)^2}$$

where $^1E_{1u},s_{1g}$ and $^3E_{1u},s_{1g}$ correspond to the energy of the lowest-energy peaks in the one- and two-photon absorption spectra (1069 nm = 1.16 eV and 1100 nm = 1.13 eV, respectively, in the case of **3**), and $^1E_{2g},s_{1g}$ corresponds to the energy gap between triplet and singlet ground states (−2.56 kcal mol^{-1} = 0.11 eV for **3**).[9b] In accord with this equation, the biradical character (y) of **3** was estimated to be 0.63. Although this estimated value deviates from that predicted to give rise to the maximum TPA performance ($y \approx 0.38$, as noted above), the actual TPA cross-section value of **3** is likely to be greater than that predicted by theory. This is because the expanded porphyrin scaffold could potentially enhance the TPA cross section as has previously been inferred in the case of a wide range of porphyrinoid systems.[24c] Nevertheless, we conclude that the inherent open-shell aromaticity of **3** plays a key role in defining the observed TPA properties (vide infra).

The effect of monoradical electronic structures, such as those that characterize **2**, on TPA performance has not been studied extensively by experiment. On the basis of theoretical studies, it is predicted that the γ values will increase with the spin multiplicity and should, again, be related to the degree of bond breaking both in neutral conjugated radicals and in radical cation(anion) species.[30] This predicted monotonic enhancement in the γ values is thought to reflect nonsymmetrical charge (electron) distributions. This has led to the suggestion that the presence of an unpaired electron can contribute to variations in the molecular polarizability. The larger γ value calculated for **2** as above is thus consistent with an enhanced probability of two-photon transitions relative to **1**. Nevertheless, this same analysis leads to the prediction that the intermediate singlet biradical character of **3** will be reflected in TPA values that are larger than those seen in the case of the monoradical **2**.

Aromaticity Effects Involving Open-Shell Electronic Configurations. As noted above, the meso-free **1** displays spectral features expected for a 26 π-electron aromatic macrocycle. In contrast, the open-shell electronic configurations of the meso-keto and diketo derivatives **2** and **3** are expected to translate not just to distinct optical properties (vide supra), but also

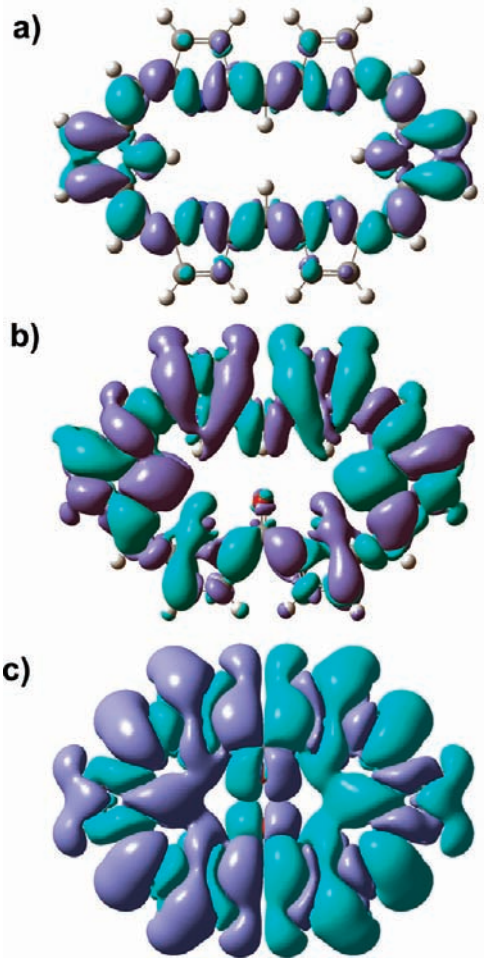

Figure 4. The γ density distribution of (a) **1**, (b) **2**, and (c) **3** calculated at the BHandHLYP/6-31G(d) approximation level without meso-aryl substituents. The purple and green solid surfaces represent the positive and negative γ densities with an isosurface of $\pm$100 au, respectively.

uncommon aromaticity effects. In general, aromatic cyclic molecules are characterized by small bond length alterations, an ability to sustain diatropic ring currents, and a high degree of electronic stabilization. On the basis of investigations involving a wide range of expanded porphyrinionds, a variety of useful theoretical methodologies have been developed for determining the degree of (anti)aromaticity in a given π-conjugated macrocyclic system; these include NICS values,[31] HOMA values,[32] and AICD plots.[33] The NICS calculation is a computational method that calculates the chemical shift of a hypothetical lithium ion positioned at a given point inside the ring. Negative and positive NICS values are thus correlated with aromaticity and antiaromaticity, respectively, with the magnitude of these values providing means by which the degree of aromaticity can be quantified.

The meso-free **1** shows a negative NICS(0)[34] of $\delta = -15.1$ ppm at the central point of the macrocycle. A slightly larger negative value of -16.1 ppm was also determined at a point offset from the center (i.e., between the flanking pyrrole rings of the tripyrran subunits). Such findings are in line with the strong aromatic nature predicted given the 26 π-electron periphery (Table 1, and Figure S8a in the Supporting Information). On the other hand, the keto derivative **2** is characterized by rather small, near-neutral NICS(0) values (center, +4.8 ppm; sides, +5.6 ppm). This is consistent with the nonaromatic character predicted for this macrocycle on the basis of its formal odd numbered 27 π-electron count (Table 1 and Figure S8b in the Supporting Information).

In contrast to **2**, negative NICS(0) values were calculated in the case of **3** (center, -8.2 ppm; sides, -4.1 ppm) (Table 1 and Figure S8c in the Supporting Information). Such findings are consistent with a degree of aromatic character. Support for this conclusion came from ^{1}H NMR spectroscopic analyses. Specifically, the spectrum of **3** recorded in CD_2Cl_2 at -80 °C revealed the presence of pyrrolic β-CH signals at relatively low field (i.e., at 8.0 and 9.6 ppm), as well as inner NH resonances in a rather shielded region, 4.5 ppm (Figure S9 in the Supporting Information).[9b] The chemical shifts of **3** bear analogy to what is seen in the case of **1** (β-CH (9.03 and 10.49 ppm) and inner NHs (-4.97 ppm)), although a weaker diatropic ring current is inferred.[9a] The theoretically estimated chemical shifts of δ_{CH} = 8.3, 7.7, and 7.6 ppm for the β-H and symmetric inner pyrrole NHs of δ_{NH} = 6.5 ppm, obtained by application of the GIAO-UB3LYP method, are in good agreement with the experimental chemical shift values. This is taken as further evidence of the partial aromatic nature of **3**. Further, a transverse NICS spectral scan of **3** revealed an enhancement in the diamagnetism at points closest to the central diketo moieties (i.e., the center of the macrocycle). This finding stands in contrast to the quasi-flat diamagnetism predicted to exist within the cavity of **1** (Figure S8 in the Supporting Information). This difference is consistent with the recovery of aromaticity observed within the central octatetraene core unit present in an oxidized corrole dimer; this latter species like **3** displays ground-state singlet biradical character.[7b]

Another method for the quantification of aromaticity involves the HOMA value, which is defined as the normalized sum of the squared deviations for the bond lengths from an optimal value. The HOMA values for the optimized structures of **1**, **2**, and **3** are 0.844, 0.731, and 0.672, respectively (Table 1 and Table S7 in the Supporting Information). Thus, the extent of aromaticity appears to decrease as the number of unpaired electrons within the macrocycle increases.[35]

Despite the above observations, it is important to appreciate that macrocycles **2** and **3** can be considered as formal 28 π-electron anitaromatic hexaphyrins, judging from the number of amine NH protons present in their respective core scaffolds. This assignment is consistent with the general features of the antiaromatic expanded porphyrins including the excited-state dynamics. For instance, it was found that the calculated HOMA values of **2** and **3** (0.731 and 0.672, respectively; vide supra) are close to those of a genuine antiaromatic vinylene-bridged [28]hexaphyrin (0.636) with a similar dumbbell-like geometry.[22a] The slight increase in the total HOMA values seen for **2** and **3** relative to this latter benchmark might reflect a degree of π-electron delocalization promoted by the unpaired radical electrons present in macrocycles **2** and **3**, which would be expected to lead to increased bond equalization.[36]

Although these open-shell compounds do not come under any existing definitions of porphyrinoid systems per Hückel's aromaticity rule, our findings, taken in concert, lead us to conclude that **2** and **3** are delocalized nonaromatic and partially aromatic molecules, respectively, that display key features consistent with the presence of antiaromatic 28 π-electron conjugated electron circuits. Alternatively, the neutral radicaloid **2** and singlet biradicaloid **3** can be regarded as formally 27 π-electron and 26 π-electron conjugated molecules containing one or two unpaired electrons, respectively, in their ground states.

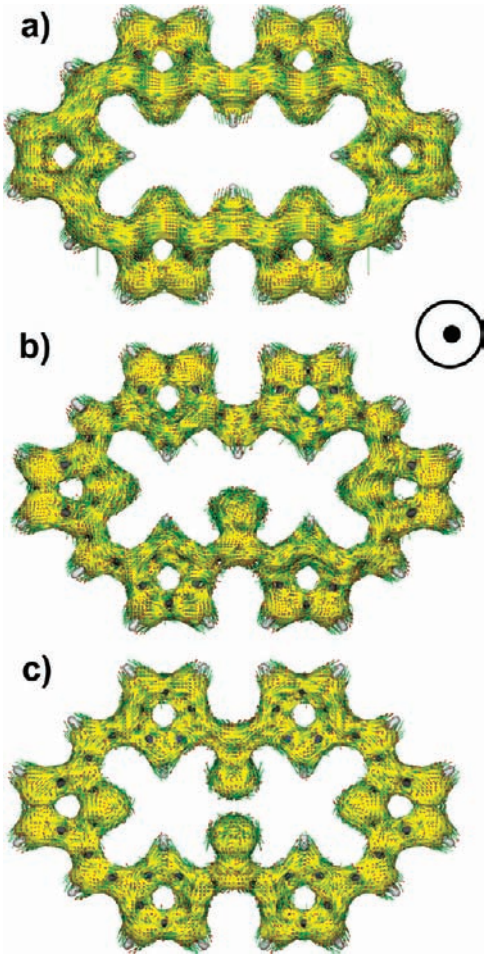

Figure 5. AICD plots of (a) **1**, (b) **2**, and (c) **3** at an isosurface value of 0.05. The external magnetic field is applied orthogonal to the macrocycle plane.

To further support our hypothesis of open-shell nonaromaticity for **2** and degree of aromaticity for **3** as suggested above, the AICD plots were constructed for **1**−**3** (Figure 5). In general, the AICD plots reveal a three-dimensional image of the delocalized electrons present in aromatic systems and have been utilized in the analysis of various planar and nonplanar porphyrinoids (in closed-shell forms).[37] Further, the AICD plots can reveal through numerous point vectors the induced ring current density expected when an external magnetic field is applied. As used here, green lines reflect the intensity, and the red conics indicate the direction of the ring current. The proper conjugation pathways can then be estimated upon application of an external magnetic field by controlling the isosurface values. The AICD isosurface plot of **1** indicates a strong ring current and a well-delocalized topology along with the 26 π-electron network, as would be expected given its aromatic character and highly symmetric structure. The current density vectors mapped onto the ACID isosurface plot of **1** exhibit a clockwise current flow and a distinct pathway (Figure 5a and Figure S10 in the Supporting Information). In contrast, the AICD isosurface plot of **2** reveals a relatively poor electron conjugation with an appearance of disrupted patterns within the electronic current. This makes it difficult to assign each of the alternate single and double bond relays within the topological conjugation pathway (Figure 5b and Figure S11 in the Supporting Information). Nevertheless, in general terms, the AICD plots are in agreement with the small positive NICS(0) values noted above. They thus provide support for the proposed nonaromatic (or antiaromatic) character of **2**. A counterclockwise current flow was also observed in the plot of **2** based on the direction of the current vectors. This paratropic ring current might be ascribed to the intrinsic paramagnetic property induced by the open-shell configuration, as well as the antiaromatic-like parity that would be expected given the cyclic conjugation of **2**.

The most intriguing feature of the AICD plot of **3** is the presence of a net clockwise (diamagnetic) current density flow. This is true even though the AICD isosurface plot of **3** reflects a reduced level of connectivity in the current density map as compared to **1** (Figure 5c and Figure S12 in the Supporting Information). Further inspection of the AICD plots reveals a counter clockwise current within the macrocycle, along with an overall stronger clockwise current that runs along the outside of the macrocycle (Figure S12g in the Supporting Information). Thus, the AICD plot of **3** is thought to reflect a recovery of aromaticity despite the formal 28 π-electron antiaromatic conjugated network in the core. This current density map of **3** suggests the presence of so-called double (mixed) aromaticity. Double aromaticity generally arises from the presence of two orthogonal, cyclically delocalized electronic systems within a single macrocycle. This phenomenon, including mixed aromatictiy, has been observed previously in the case of certain [4*n*]annulene systems in the triplet state.[38] In the case of **3**, the overall clockwise diatropic ring current is consistent with an aromatic system associated with the open-shell electronic configuration, while the minor counter clockwise paratropic current is thought to reflect the intrinsic antiaromatic nature of this hexaphryin. Therefore, two independent ring currents coexist in **3**, which arise from a mixing of π-orbitals.

Reduction of the Antiaromaticity of 4 via Structural Perturbation of the π-Conjugation Pathway. The presence of the bridging carbonyl groups at the meso positions in **2** and **3** could contribute to an interruption of the overall macrocyclic π-conjugation pathway of the corresponding [28]hexaphyrins. To allow for a proper comparison, within the context of the same π conjugation pathways, the meso-free [28]hexaphyrin derivative (**4**) corresponding to the two-electron reduced form of **1** was modeled (Chart 1 and Figure S1 in the Supporting Information). According to the calculated NICS (+43.1 ppm) and HOMA values (0.653) for the optimized structure of **4** (using the RB3LYP/6-31G** method), the π-conjugation present in **4** is attributed to a 28 π-electron conjugated periphery. To the extent this assignment is correct, it provides support for the presence of strong antiaromaticity, something that leads to an electronic configuration similar to that present in **2** and **3** (Table 1). Further, an analysis of the relevant bond distances within the congeneric series **2**−**4** reveals elongated separations in the case of **2** and **3** for the carbon−carbon bonds bridging at the meso carbonyl moiety (bond numbers: 13, 14, 27, and 28), with the calculated separations being 1.458 (13) and 1.455 Å (14) and 1.470 (13 and 27) and 1.465 Å (14 and 28) for **2** and **3**, respectively (Figure 6 and Tables S1−3 in the Supporting Information). The C−C bonds adjacent to the C=O group(s) can thus be regarded as typical C(sp^2)−C(sp^2) single bonds in both **2** and **3**.

Such a finding leads us to suggest that the separation provided by the stable isomeric keto form of the oxyallyl subunit present in **2** and **3** leads to a weakening in the overall macrocyclic

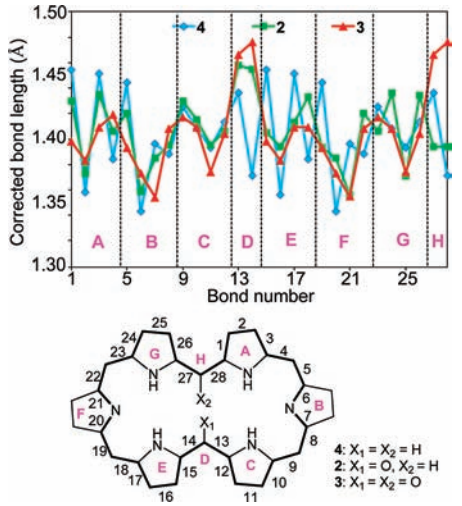

Figure 6. Comparison of the bond length distributions (top) between **4** (blue), **2** (green), and **3** (red). The corresponding number of bonds is shown in the bottom figure.

Scheme 1. Molecular Structures of (a) 3 and (c) the Oxidized Corrole Dimer, DH_2CD, with Antiaromatic-like Conjugation Pathways (Emphasized in Blue); Core Structures of (b) Hexaphyrin and (d) Cyclooctatetraene (COD) Indicate One of the Possible Biradical Resonance Structures

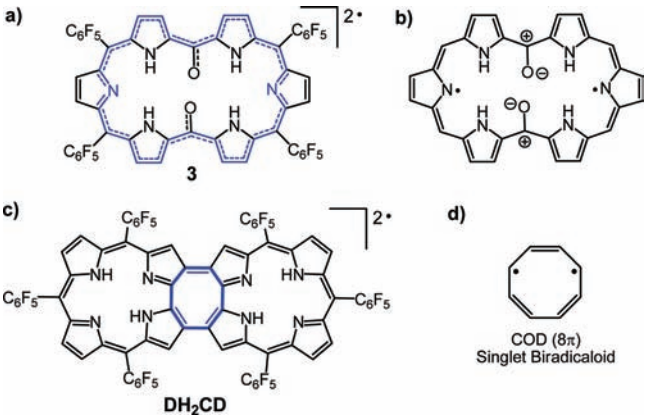

π-conjugation due to Jahn−Teller distortion.[39] As a consequence, the overall antiaromaticity expected for a formal 28 π-electron network is thus reduced in accord with the following sequence: **4** > **2** > **3**. Such a trend is in accord with the theoretical analyses discussed above.

In the case of **3**, where significant aromatic character is inferred, the meso-carbonyl groups also contribute to the origin of the singlet biradical nature, as deduced from the orbital correlation diagrams for **3** (Figure S13 in the Supporting Information). The distribution of singly occupied molecular orbitals (SOMOs) of both flanking tripyrrane radical units is quite similar to those of each HSOMO of the α- and β-spin orbitals of **3** by BS-UB3LYP calculations (Figure S6 in the Supporting Information). Thus, the molecular orbitals of **3** can be considered to be derived from symmetric and antisymmetric mixings of the SOMOs of the isolated tripyrrane radical subunits that are linked by carbonyl groups, respectively. The carbonyl groups serve to interrupt much of the macrocyclic π-conjugation that would otherwise be expected in the case of **3** and that would give rise to overall 28 π-electron antiaromaticity. In other words, the high relative stability of the keto form of **3** stabilizes the open-shell electronic configuration and gives rise to partial aromatic character as has been seen for other singlet biradical molecules.[5]

IV. SUMMARY

In this study, the geometrical, vibrational, and photophyscial properties of a series of meso-free hexaphyrin derivatives, **1**−**3**, have been comparatively examined. These analyses, along with supporting theoretical calculations, provide support for the conclusion that both the neutral radicaloid **2** and the singlet biradicaloid **3** exhibit unique ground-state electronic structures, specifically with one-photon forbidden states as the lowest excited state. It was found that the low-lying optically forbidden states associated with the open-shell electron configurations play an important role in the overall photophysical properties. In addition, both **2** and **3** displayed enhanced TPA cross sections relative to **1**, with the largest value being seen for **3**. The TPA profiles of **1**−**3** were well assessed by the aid of second hyperpolarizability, γ calculations.

On the basis of the experimental and theoretical results, the radicaloid **2** and singlet biradicaloid **3** were considered to be nonaromatic and partially aromatic species, respectively. In the case of **2**, the net nonaromaticity is easily understood in terms of the odd number of π-electrons intrinsic to its 27 π-electron conjugated circuit, although such a system cannot be categorized according to classic aromaticity rules. The aromatic character of **3** was inferred from the negative NICS(0) value at the center of macrocycle. It is also seen in the characteristic shifts observed in the ^{1}H NMR spectrum, which are ascribed to an aromatic ring current effect as noted in the AICD map.

The bridging keto moieties present in macrocycles **2** and **3** are thought to play a key role in stabilizing the observed neutral radicaloid and singlet biraidicaloid species, respectively; the presence of these groups and the associated radical forms also contributes to the overall aromatic stabilization energy, particularly in the case of **3**.

System **3** differs from a previous system with ground-state singlet biradicaloid character, the oxidized corrole dimer (**DH_2CD**) (Scheme 1).[7] This latter structure contains a planar, antiaromatic 8 π-cyclooctatetraene (COD) linker between the oxidized corrole rings. In **DH_2CD**, evidence of distinct aromaticity is seen for the central COD moiety, as inferred from the negative NICS value (−4.31 ppm). As in the case of **3**, the observed aromaticity reflects a contribution from singlet biradical forms. The biradical form of **3** serves to stabilize explicitly what is a 26 π-electron aromatic pathway within a 28 π-conjugated network. To the best of our knowledge, this is the first systematic investigation of ground-state open-shell aromaticity and photophysical properties within a congeneric set of porphyrinoids. The findings reported herein are expected to be general and lead us to predict that formally antiaromatic systems with $[4n]\pi$-electron pathways that also possess open-shell biradical electronic configurations may display aromatic character in their respective singlet ground states.[40]

■ ASSOCIATED CONTENT

Supporting Information. Detailed experimental FTIR, *z*-scan traces, vertical transition, MO energy diagram, NICS scan,

AICD calculations, and complete refs 13, 15, and 26. This material is available free of charge via the Internet at http://pubs.acs.org.

AUTHOR INFORMATION

Corresponding Author
sessler@mail.utexas.edu; osuka@kuchem.kyoto-u.ac.jp; dongho@yonsei.ac.kr

ACKNOWLEDGMENT

This research was supported by the Midcareer Researcher (2010-0029668) and WCU (World Class University) programs (R32-2010-000-10217-0) through the National Research Foundation of Korea funded by the Ministry of Education, Science and Technology (MEST), and an AFSOR/AOARD grant (no. FA2386-09-1-4092). The work at Kyoto University was financially supported by Grants-in-Aid for Scientific Research (nos. 22245006 and 20108001 "pi-Space") from MEXT of Japan. Support from the National Science Foundation (grant no. CHE 105790 to J.L.S.) and the Robert A. Welch Foundation (grant F-1018 to J.L.S.) is also gratefully acknowledged. We strongly acknowledge Prof. Dr. M. Nakano (Osaka University) and Dr. K. Saita (Sophia University) for their help and advice with the second hyperpolarizability calculations. The theoretical calculations were performed by using the supercomputing resource of the Korea Institute of Science and Technology Information (KISTI).

REFERENCES

(1) (a) Boldyrev, A. I.; Wang, L.-S. *Chem. Rev.* **2005**, *105*, 3716. (b) Chen, Z.; King, R. B. *Chem. Rev.* **2005**, *105*, 3613. (c) Rzepa, H. S.; Chen, R. *Chem. Rev.* **2005**, *105*, 3697. (d) Lu, X.; Chen, Z. *Chem. Rev.* **2005**, *105*, 3643. (e) Yoon, Z. S.; Osuka, A.; Kim, D. *Nat. Chem.* **2009**, *1*, 113. (f) Osuka, A.; Saito, S. *Chem. Commun.* **2011**, *47*, 4330. (g) Stępień, M.; Sprutta, N.; Latos-Grażyński, L. *Angew. Chem., Int. Ed.* **2011**, *50*, 4288. (h) Saito, S.; Osuka, A. *Angew. Chem., Int. Ed.* **2011**, *50*, 4342.

(2) Garratt, P. J. *Aromaticity*; Wiley: New York, 1986.

(3) Baird, N. C. *J. Am. Chem. Soc.* **1972**, *94*, 4941.

(4) (a) Möllerstedt, H.; Piqueras, M. C.; Crespo, R.; Ottosson, H. O. *J. Am. Chem. Soc.* **2004**, *126*, 13938. (b) Gogonea, V.; Schleyer, P. v. R.; Schreiner, P. R. *Angew. Chem., Int. Ed.* **1998**, *37*, 1945. (c) Fowler, P. W.; Steiner, E.; Jennesken, L. W. *Chem. Phys. Lett.* **2003**, *371*, 719. (d) Sonicini, A.; Fowler, P. W. *Chem. Phys. Lett.* **2008**, *450*, 431. (e) Ottosson, H.; Kilså, K.; Chajara, K.; Piqueras, M. C.; Crespo, R.; Kato, H.; Muthas, D. *Chem.-Eur. J.* **2007**, *13*, 6998.

(5) (a) Bendikov, M.; Duong, H. M.; Starkey, K.; Houk, K. N.; Carter, E. A.; Wudl, F. *J. Am. Chem. Soc.* **2004**, *126*, 7416. (b) Konishi, A.; Hirao, Y.; Nakano, M.; Shimizu, A.; Botek, E.; Champagne, B.; Shiomi, D.; Sato, K.; Takui, T.; Matsumoto, K.; Kurata, H.; Kubo, T. *J. Am. Chem. Soc.* **2010**, *132*, 11021. (c) Kubo, T.; Shimizu, A.; Sakamoto, M.; Uruichi, M.; Yakushi, K.; Nakano, M.; Shiomi, D.; Sato, K.; Takui, T.; Morita, Y.; Nakasuji, K. *Angew. Chem., Int. Ed* **2005**, *44*, 6564. (d) Kubo, T.; Shimizu, A.; Uruichi, M.; Yakushi, K.; Nakano, M.; Shiomi, D.; Sato, K.; Takui, T.; Morita, Y.; Nakasuji, K. *Org. Lett.* **2007**, *9*, 81. (e) Shimizu, A.; Uruichi, M.; Yakushi, K.; Matsuzaki, H.; Okamoto, H.; Nakano, M.; Hirao, Y.; Matsumoto, K.; Kurata, H.; Kubo, T. *Angew. Chem., Int. Ed.* **2009**, *48*, 5482–5486.

(6) Zipse, H. *Top. Curr. Chem.* **2006**, *263*, 163.

(7) (a) Hiroto, S.; Furukawa, K.; Shinokubo, H.; Osuka, A. *J. Am. Chem. Soc.* **2006**, *128*, 12380. (b) Cho, S.; Lim, J. M.; Hiroto, S.; Kim, P.; Shinokubo, H.; Osuka, A.; Kim, D. *J. Am. Chem. Soc.* **2009**, *131*, 6412. (c) Ishida, M.; Karasawa, S.; Uno, H.; Tani, F.; Naruta, Y. *Angew. Chem., Int. Ed.* **2010**, *49*, 5906.

(8) Rath, H.; Tokuji, S.; Aratani, N.; Furukawa, K.; Lim, J. M.; Kim, D.; Shinokubo, H.; Osuka, A. *Angew. Chem., Int. Ed.* **2010**, *49*, 1489.

(9) (a) Koide, T.; Kashiwazaki, G.; Suzuki, M.; Furukawa, K.; Yoon, M.-C.; Cho, S.; Kim, D.; Osuka, A. *Angew. Chem., Int. Ed.* **2008**, *47*, 9661. (b) Koide, T.; Furukawa, K.; Shinokubo, H.; Shin, J.-Y.; Kim, K. S.; Kim, D.; Osuka, A. *J. Am. Chem. Soc.* **2010**, *132*, 7246.

(10) The less sterically hindered meso-aryl-substituted [26]hexaphyrin (e.g.; 5,20-bis(3-thenyl)-10,15,25,30-tetrakis(pentafluorophenyl)-substituted [26]hexaphyrin) adopts a dynamic type I conformation. See: Suzuki, M.; Osuka, A. *Chem.-Eur. J.* **2007**, *13*, 196.

(11) Meso-substituted hexaphyrins afford meso-oxygenated products when adventitious water is incorporated as an oxygen atom source during the metalation reaction. See: (a) Shimizu, S.; Anand, V. G.; Taniguchi, R.; Furukawa, K.; Kato, T.; Yokoyama, T.; Osuka, A. *J. Am. Chem. Soc.* **2004**, *126*, 12280. (b) Mori, S.; Shimizu, S.; Shin, J.-Y.; Osuka, A. *Inorg. Chem.* **2007**, *46*, 4374. In contrast, the oxygenation of meso-free **1** is thought to involve molecular oxygen as the oxygen atom source. See:(c) Koide, T.; Kashiwazaki, G.; Furukawa, K.; Osuka, A. *Inorg. Chem.* **2009**, *48*, 4595.

(12) Makarov, N. S.; Drobizhev, M.; Rebane, A. *Opt. Express* **2008**, *16*, 4029.

(13) Pople, J. A.; et al. *Gaussian 03*, revision B.05; Gaussian, Inc.: Pittsburgh, PA, 2003.

(14) (a) Becke, A. D. *Phys. Rev. A* **1988**, *38*, 3098. (b) Lee, C.; Yang, W.; Parr, R. G. *Phys. Rev. B* **1988**, *37*, 785.

(15) Ohta, S.; Nakano, M.; et al. *J. Phys. Chem. A* **2007**, *111*, 3633.

(16) The relatively larger transmission bands around 1500 cm^{-1} can be assigned as the aromatic C−C bond stretching and C−N stretching modes, because these bands are not significantly shifted by a comparison with those of the derivatives including all meso-pentafluorophenel-substituted [26]hexaphyrin; see Figure S3 in the Supporting Information.

(17) Lahaye, D.; Muthukumaran, K.; Hung, C.-H.; Gryko, D.; Rebouças, J. S.; Spasojević, I.; Batinić-Haberle, I.; Lindsey, J. S. *Bioorg. Med. Chem.* **2007**, *15*, 7066.

(18) The overestimation of the corresponding energy of frequencies of the carbonyl stretching bands is due to the replacement of the meso-pentafluorophenyl groups with simple hydrogen atoms.

(19) Ahn, T. K.; Kwon, J. H.; Kim, D. Y.; Cho, D. W.; Jeong, D. H.; Kim, S. K.; Suzuki, M.; Shimizu, S.; Osuka, A.; Kim, D. *J. Am. Chem. Soc.* **2005**, *127*, 12856.

(20) While the deficiency in the long-range behavior of the potential associated with the hybrid B3LYP functional leads to an underestimation of the transition energies by the TD-B3LYP method, the unrestricted TD-DFT method is a still promising approach for open-shell systems with larger structures (i.e., singlet biradicals) and can be used to simulate the absorption spectra. See: Fabian, J. *Dyes Pigm.* **2010**, *84*, 36.

(21) Gouterman, M. In *The Porphyrins*; Dolphin, D., Ed.; Academic Press: New York, 1987; Vol. III, Part A, pp 1−165.

(22) (a) Yoon, M.-C.; Cho, S.; Suzuki, M.; Osuka, A.; Kim, D. *J. Am. Chem. Soc.* **2009**, *131*, 7360. (b) Cho, S.; Yoon, Z. S.; Kim, K. S.; Yoon, M.-C.; Cho, D.-G.; Sessler, J. L.; Kim, D. *J. Phys. Chem. Lett.* **2010**, *1*, 895. (c) Shin, J.-Y.; Kim, K. S.; Yoon, M.-C.; Lim, J. M.; Yoon, Z. S.; Osuka, A.; Kim, D. *Chem. Soc. Rev.* **2010**, *39*, 2751.

(23) The similar phenomenon could be observed in Ni(II), Co(II) tetrapyrrole complexes and Zn(II) porphyrin cation radical species. The fast decay of excited states into the ground state resulted from the effective vibronic mixing of the d-orbitals of metal centre and π orbitals of the ligands. Thus, the excited-state dynamics of **2** and **3** will differ from the original ground-state spectrum slightly because of the electronic interactions imparted by the unpaired radical electrons similar to their open-shell electronic structures of transition metal complexes. See: (a) Okhrimenko, A. N.; Gusev, A. V.; Rodgers, M. A. J. *J. Phys. Chem. A* **2005**, *109*, 7653. (b) Zamyatin, A. V.; Soldatova, A. V.; Rodgers, M. A. J. *Inorg. Chim. Acta* **2007**, *360*, 857. (c) Rajapakse, G. V. N.; Soldatova, A. V.; Rodgers, M. A. J. *J. Phys. Chem. B* **2010**, *114*, 14205 and references therein.

(24) (a) Kim, K. S.; Lim, J. M.; Osuka, A.; Kim, D. *J. Photochem. Photobiol., C* **2008**, *9*, 13. (b) Pawlicki, M.; Collins, H. A.; Denning, R. G.;

Anderson, H. L. *Angew. Chem., Int. Ed.* **2009**, *48*, 3244. (c) Lim, J. M.; Yoon, Z. S.; Shin, J.-Y.; Kim, K. S.; Yoon, M.-C.; Kim, D. *Chem. Commun.* **2009**, 261. (d) He, G. S.; Tan, L.-S.; Zheng, Q.; Prasad, P. N. *Chem. Rev.* **2008**, *108*, 1245.

(25) Kamada, K.; Ohta, K.; Kubo, T.; Shimizu, A.; Morita, Y.; Nakasuji, K.; Kishi, R.; Ohta, S.; Furukawa, S.; Takahashi, H.; Nakano, M. *Angew. Chem., Int. Ed.* **2007**, *46*, 3544.

(26) (a) Ohta, S.; Nakano, M.; et al. *Chem. Phys. Lett.* **2006**, *420*, 432. (b) Nakano, M.; et al. *J. Phys. Chem. A* **2007**, *111*, 9102. (c) Nakano, M.; et al. *J. Phys. Chem. Lett.* **2011**, *2*, 1094.

(27) (a) Nakano, M.; Nitta, T.; Yamaguchi, K.; Champagne, B.; Botek, E. *J. Phys. Chem. A* **2004**, *108*, 4105. (b) Nakano, M.; Kishi, R.; Nitta, T.; Kubo, T.; Nakasuji, K.; Kamada, K.; Ohta, K.; Champagne, B.; Botek, E.; Yamaguchi, K. *J. Phys. Chem. A* **2005**, *109*, 885. (c) Bonness, S.; Fukui, H.; Yoneda, K.; Kishi, R.; Champagne, B.; Botek, E.; Nakano, M. *Chem. Phys. Lett.* **2010**, *493*, 195.

(28) (a) Nakano, M.; Kishi, R.; Ohta, S.; Takahashi, H.; Kubo, T.; Kamada, K.; Ohta, K.; Botek, E.; Champagne, B. *Phys. Rev. Lett.* **2007**, *99*, 033001.

(29) Kamada, K.; Ohta, K.; Shimizu, A.; Kubo, T.; Kishi, R.; Takahashi, H.; Botek, E.; Champagne, B.; Nakano, M. *J. Phys. Chem. Lett.* **2010**, *1*, 937.

(30) (a) Qiu, Y.-Q.; Fan, H.-L.; Sun, S.-L.; Liu, C.-G.; Su, Z.-M. *J. Phys. Chem. A* **2008**, *112*, 83. (b) Li, Z.-J.; Li, Z.-R.; Wang, F.-F.; Ma, F.; Chen, M.-M.; Huang, X.-R. *Chem. Phys. Lett.* **2009**, *468*, 319.

(31) Chen, Z.; Wannere, C. S.; Corminboeuf, C.; Puchta, R.; Schleyer, P. V. R. *Chem. Rev.* **2005**, *105*, 3842.

(32) Krygowski, T. M.; Cyrański, M. K. *Chem. Rev.* **2001**, *101*, 1385.

(33) Geuenich, D.; Hess, K.; Köhler, F.; Herges, R. *Chem. Rev.* **2005**, *105*, 3758.

(34) The termed NICS(0) was based on the total isotropic shielding computed at ring centers (0 Å). It has been known that most of the NICS(0) values at noncentral points at a distance of ~1 Å from adjacent C or N atoms are slightly larger than those at central positions due to the perturbation of local magnetic effects arising from a proximity to the π-electronic conjugation pathway. The overall geometries of all derivatives, however, maintain the dumbbell-like conformation as the main conformer due to larger conformational stability: Cyrañski, M. K.; Krygowski, T. M.; Wisiorowski, M.; Hommes, N. J. R. v. E.; Schleyer, P. v. R. *Angew. Chem., Int. Ed.* **1998**, *37*, 177.

(35) The HOMA values calculated from the X-ray crystal structures proved qualitatively similar to those derived by using the optimized geometries except in the case of **2**. Here, the deviation is ascribed to an intriguing crystal packing observed in the case of the radical dimer of **2** (Table S7 and Figure S2 in the Supporting Information).

(36) Rosokha, S. V.; Kochi, J. K. *J. Org. Chem.* **2006**, *71*, 9357.

(37) (a) Yoon, M.-C.; Shin, J.-Y.; Lim, J. M.; Saito, S.; Yoneda, T.; Osuka, A.; Kim, D. *Chem.-Eur. J.* **2011**, *17*, 6707. (b) Higashino, T.; Lim, J. M.; Miura, T.; Saito, S.; Shin, J.-Y.; Kim, D.; Osuka, A. *Angew. Chem., Int. Ed.* **2010**, *49*, 4950. (c) Lee, J. S.; Lim, J. M.; Toganoh, M.; Furuta, H.; Kim, D. *Chem. Commun.* **2010**, *46*, 285.

(38) (a) Bean, D. E.; Fowler, P. W.; Soncini, A. *Chem. Phys. Lett.* **2009**, *483*, 193. (b) Fowler, P. W.; Mizoguchi, N.; Bean, D. E.; Havenith, R. W. A. *Chem.-Eur. J.* **2009**, *15*, 6964.

(39) Bonačić-Koutecký, V.; Koutecký, J.; Michl, J. *Angew. Chem., Int. Ed. Engl.* **1987**, *26*, 170.

(40) Although the extent of aromaticity in the singlet biradical molecules is likely to be dependent on the distinct molecular structure, the reduction of antiaromaticy in what are formally antiaromatic macrocycles (e.g., phenalenyl-radical dimer) is thought to reflect the presence of accessible ground-state singlet biradicaloid states. It is noteworthy that the [4*n*] antiaromatic pentalene (8 π-electrons) and *s*-indacene (12 π-electrons) also display singlet biradical properties in their respective ground states; see ref 27c.